Surface Etching and Temperature Effects on SiC Electroluminescence

Surface Etching and Temperature Effects on SiC Electroluminescence

By Liam Dow,

A Thesis Submitted to the School of Graduate Studies in the Partial Fulfillment of the Requirements for the Degree Master of Applied Science

McMaster University

Master of Applied Science (2024)

Hamilton, Ontario (Department of Engineering Physics)

TITLE: Surface Etching and Temperature Effects on SiC Electroluminescence

AUTHOR: Liam Dow (McMaster University)

SUPERVISOR: Dr. Adrian Kitai

NUMBER OF PAGES: xv, 63

Abstract

Silicon carbide was the first substance reported to display electroluminescence and enabled the first blue light emitting diode (LED). While the challenges of fabrication and poor efficiency lead to alternatives being developed, recent demand for high temperature, high power electronics have brought silicon carbide back to the forefront of development and improved quality and production scale.

Due to the large bandgap, it is possible for light across the visible spectrum and into ultraviolet (UV) to be emitted. The wavelength of light produced depends heavily on the inclusion of different defects and impurities. Great care is taken to minimize this to improve device performance. The ability to induce and control these defects however, could allow for a range of wavelengths to be emitted and enable different colours of LEDs or the creation of white LEDs without the need for phosphors.

This thesis explores different post fabrication treatments and operating conditions that can be used to alter the luminescent intensity and spectrum of commercial devices. Chapter one will include a brief history of LED development in addition to exploring the strengths and weaknesses of silicon carbide as a light emitting material. The following chapter will cover the theory behind LED operation and the structure/properties of SiC.

In chapter 4, an electrochemical etch is used to alter the emission spectrum through the formation of a nano-porous surface layer. The processed device is then used to demonstrate electroluminescence due to lateral charge diffusion in SiC for the first time.

Chapter 5 details the effects of operating conditions on electroluminescence with a strong focus on temperature, and chapter 6 suggests future work and possible applications.

Acknowledgements

Completion of my graduate studies would not have been possible without the contribution and assistance of all those that supported me.

Thank you to my supervisor, Dr. Kitai, whose patience and understanding are second to none, and whose expertise and guidance was vital to the completion of this work.

My friends, you never fail to pull me up from my low points, I would not have come this far without your belief and encouragement.

My family, you're unending love and support is the foundation for all of my accomplishments.

Thank you.

Contents

List of Figures

List of Tables

Acronyms

DDCT diffusion-driven charge transport

IR infrared

LCD liquid crystal display

LED light emitting diode

MOCVD metalorganic chemical vapour deposition

PTFE Polytetrafluoroethylene

RIE reactive ion etching

UV ultraviolet

Chapter 1

Introduction

1.1 light emitting diode (LED) History

The first recorded observation of electroluminescence was made as long ago as 1907 by H.J Round while investigating the electrical properties of silicon carbide (Known then as carborundum).[1] He wrote "On applying a potential of 10 volts between two points on a crystal of carborundum, the crystal gave out a yellowish light." When doing the same but with 110 volts, he observed orange, green, and blue light in addition to yellow.

Further work was done on luminescent silicon carbide during the 1920s by soviet scientist O.V. Losev.[2] However the efficiency of light emission was so poor that it was not suitable as a commercial device. It was not until 1962 that a practical LED was achieved and patented by Baird and Pittman while working at Texas Instruments.[3] With this patent, Texas Instruments began manufacturing the first commercially available LED. The device was made of gallium arsenide and emitted infrared light at a wavelength of $890\mu m$.[4]

Visible LEDs followed the development of infrared (IR) LEDs and by the end of the 1960s, multiple manufacturers and countries were producing red and green LEDs.[5]

1.2 Blue LEDs

While red, green, and IR LEDs were realized in quick succession, efficient and practical blue emission remained elusive. Initial research focused on high bandgap semiconductors such as ZnSe, however, light emission from these materials was very inefficient due to their indirect bandgap. GaN showed promise as a wide direct bandgap semiconductor but came with its own seemingly insurmountable challenges such as doping and growth of large high quality crystals. The later was overcome with the development of new fabrication technologies like metalorganic chemical vapour deposition (MOCVD). MOCVD enabled polycrystalline AlN grown on a sapphire substrate which could then subsequently be heated and used as a substrate to grow GaN. GaN grown using this method initially has a high density of dislocations but becomes much more uniform after a few microns of layer thickness. This method allowed for high quality device-grade GaN with a uniform surface finish to be grown for the first time.[5] This process was improved upon by Nakamura et al [6] in 1993 who developed a method to replace the AlN buffer layer with a low temperature GaN layer and used this high quality GaN to create a blue LED with an output power of nearly 10 times that of conventional SiC LEDs. With further developement, this 10 times difference grew to over 1000 times and rendered SiC impractical for LED applications.

1.3 White LEDs

The impact that efficient high brightness blue LEDs have had on our world is hard to overstate. Blue LEDs held the key to realising solid-state lighting for both general illumination applications and display technologies.

Blue light is higher in energy compared to other colours (red, yellow, green) and can be down-converted into these lower energy colours using phosphors. In this way, a single blue LED and a variety of phosphors can be used to create visible light of any colour. More importantly, a combination of phosphors can be used to fill out the optical spectrum resulting in white light emission.[7]

Though it is also possible to create white light simply by mixing the light from red, green, and blue LEDs together, the phosphor-converted white (PC-White) LEDs described above are often more practical for general lighting due to cost and complexity. Different colours of LEDs undergo different efficiency and hue shifts due to temperature/operating current. This means that a white LED composed of three different colour LEDs potentially requires current/temperature control circuits for each LED to ensure that the overall light output is still perceived as white. This added complexity is often more detrimental than efficiency loss during phosphor conversion. In addition, The efficiency of blue LEDs has exceed other colours especially those in the green/yellow region to the point where the process of converting blue light using a phosphor is comparable or more efficient than using an independent LED.[7] This efficiency discrepancy can be seen in Figure 1.1.

The development of white LEDs has provided high efficiency alternatives to

incandescent and compact fluorescent bulbs. Beyond improving efficiency in existing lighting applications, blue LEDs have enabled new technologies as well. The most prevalent use of LEDs today are in displays. The use of LEDs as backlights for liquid crystal display (LCD)s made mobile devices possible due to their small form factor and comparatively low heat generation. As technology has matured, the use of LEDs has expanded to larger displays such as TVs and monitors as well as ultra-large displays (Billboards) which are becoming increasingly common as price reduces.[7]

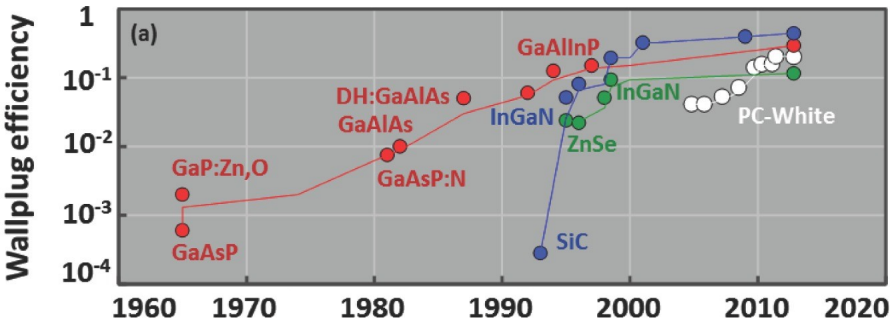

Figure 1.1: Efficiency of commercial LEDs over time comparing red, green, blue, and PC-white (Phosphor converted white light). From [7].

1.4 Silicon Carbide Luminescence

Silicon carbide has long attracted attention as a semiconductor material due to its impressive physical and electrical properties. In fact, the first observation of electroluminescence was in silicon carbide as far back as 1907.[1] Silicon carbide showed promise due to its large bandgap and ability to emit light across the visible spectrum, with blue light being of most interest. Prior to the development of high efficiency GaN LEDs by Nakamura *et al.* [6], commercially available blue LEDs and ultraviolet (UV) photodiodes were made out of silicon carbide. SiC could be

readily doped both p- and n-type and could be fabricated into viable devices with the methods available at the time. In addition, stability of SiC LEDs was much better with only 15% degradation after 10,000 hours compared to 40% degradation in GaP LEDs. This stability was attributed to the low dopant diffusivity and overall chemical inertness of silicon carbide.[8] The benefits of using SiC to emit light were overshadowed by the efficiency of the devices. In 1993 blue SiC LEDs were commercially available from Cree Research had an efficiency of 0.02-0.03% and were the most efficient available at the time.[8] The development of GaN LEDs rendered these low efficiency SiC devices largely obsolete.

In more recent years, light emission from silicon carbide has regained some attention. White light emission from SiC without phosphors was demonstrated in 2017 by Lu *et al.* [9]. This was achieved by combining the yellow photoluminescence of bulk SiC with the blue-green luminescence emitted from a porous surface layer of SiC fabricated through anodic oxidation.[9] This serves to show that SiC light emission has opportunities for improvement.

1.5 Silicon Carbide Fabrication

While the base components of silicon carbide, silicon and carbon, are both cheap and abundant, naturally occurring silicon carbide is extremely rare. Silicon carbide was actually manufactured (carborundum) before it was discovered in nature (moissanite) and as such, all silicon carbide used in electronics must be synthesized. By the time transistors entered the market, the value and potential of silicon carbide was already understood. Fabrication of large high quality silicon carbide substrates proved to be a substantial roadblock.[10]

Fabrication of single crystal SiC requires much more extreme conditions than for silicon. This is largely due to the stability of SiC at high temperatures coupled with the fact that SiC does not have a liquid phase at atmospheric pressure.

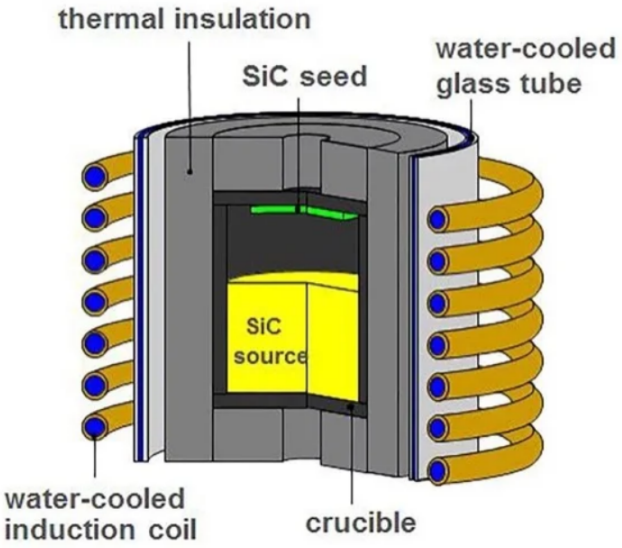

Figure 1.2: Basic schematic for growing single crystal SiC through the sublimation of SiC powder.[10]

The process to grow SiC crystals involves inductively heating source material (silicon carbide powder) in a graphite crucible to temperatures over 2200 K. At this temperature, the source material at the bottom of the crucible will sublimate. A seed crystal of SiC is suspended above the sublimating powder and kept at a lower temperature. As the vapour contact this colder seed crystal, it will deposit onto it following the same crystallographic orientation as the seed crystal. Because of this, the purity and uniformity of the seed crystal is of great importance as any crystal defects will be repeated and will extend into the new growth. The seed crystal is often taken from the best quality material of previous growth cycles.[10] Figure 1.2 shows the equipment setup involved in such a process while Figure 1.3 shows the importance of a quality seed crystal in SiC growth.

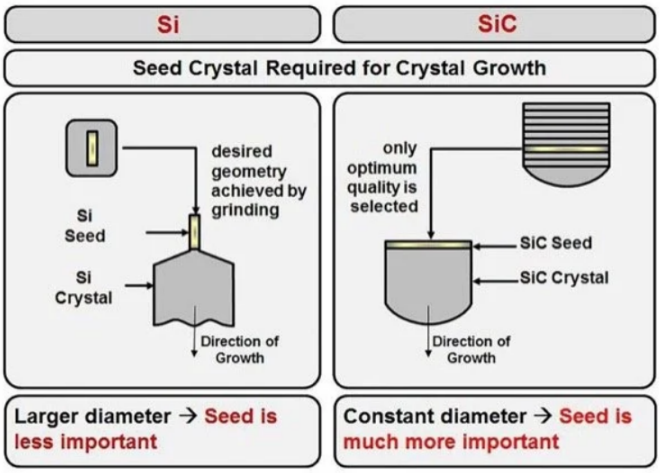

Figure 1.3: Comparison of impact and importance of the seed crystal used in the growth of silicon vs silicon carbide.[10]

The resulting ingot or boule of SiC can then be ground to the desired diameter, marked to show crystal orientation, and sliced into individual wafers which are cleaned and polished. These steps are similar to the fabrication of silicon wafers though any cutting or grinding steps are slower and cause more wear of on tools in addition to requiring diamond blades due to the extreme hardness of SiC.

1.6 Benefits of Silicon Carbide

With years of research and existing infrastructure for fabricating silicon devices, any deviation from industry standard materials or processes must have a significant value proposition in terms of manufacturing cost or device performance. Silicon carbide is more difficult and expensive to fabricate but is still attracting attention as an alternative to silicon in certain applications due to the significant device performance increase. In some applications, SiC is not only a replacement for silicon but enables applications that silicon is not suitable for.

Table 1.1: Material properties of Si and 4H-SiC at 300 K. Adapted from [12]

Property	**Si**	**4H-SiC**
Bandgap E_g (eV)	1.12	3.26
Breakdown Field (10^6V cm^{-1})	0.3	2.8
Relative permittivity	11.8	10
Thermal Conductivity λ (W cm^{-1} K)	1.5	4.9
Electron mobility (cm^2/Vs)	1400	$\parallel$ c axis: 1200 $\perp$ c axis: 1000
Electron saturation velocity V_{sat} (10^7 cm s^{-1})	1	2

SiC has a breakdown field strength that is 10 times larger than silicon as well as much higher thermal conductivity, electron velocity, and bandgap. SiC is able to operate at high temperatures without degradation than silicon. In addition, SiC is able to more efficiently transfer heat allowing for better cooling and lower temperatures at comparable powers. The increased breakdown field strength enables higher voltage operation as well as significantly thinner active drift layers when compared to silicon. [11]

1.7 SiC - An Immature Technology

Silicon carbide optimization and manufacturing scale is still in its infancy when compared to silicon. While SiC offers increased performance at higher powers and switching frequency, devices can also cost substantially more than their silicon counterpart (assuming a silicon alternative is available). This price discrepancy should shrink significantly as new production methods are developed and mass adoption spurs scaling fabrication and the economy of scale benefits that come

with it. Wolfspeed, Inc. is an industry leader in SiC and is rapidly expanding its manufacturing ability. They have begun construction on a SiC material manufacturing facility scheduled for completion in 2024 and costing roughly $1.3 billion. This facility will produce 200 mm wafers compared to the 150 mm wafers that were previously standard. This diameter increase represents a 1.7 times increase in wafer area enabling more devices to be fabricated from each wafer.[13]

In addition to this SiC material factory, Wolfspeed has also opened the first SiC fabrication facility for 200 mm wafers.[14] These two facilities when fully operational will supply high quality SiC substrate and also high performance devices at a much larger scale than previously seen. This large investment shows that industry leaders believe that the market for SiC electronics has plenty of room to expand, particularly with the steep popularity increase of electric cars.

1.8 Research Objectives

The objective of this thesis is to identify and investigate post manufacturing treatments that could increase the efficiency of light emission from commercial SiC devices. The ability of these processes to alter emission spectrum is also of interest. The hope is that these processes could result in commercially viable SiC based LEDs as the cost of SiC devices decreases due to increased use in power electronics and advances in large scale fabrication.

Chapter 2

Theory

2.1 Semiconductors

2.1.1 Band Theory

Semiconductors have undeniably shaped our modern world and it is the behavior of the electrons within them that has enabled this. Of particular importance is how electrons are arranged in solids into so called 'bands'

An atom's electrons occupy distinct energy levels and must be in their own unique energy state in order to satisfy the Pauli exclusion principle. When an atom is included in a crystal and is in close proximity to its neighboring atoms, the orbitals of the outer or valence electrons can overlap and allow electrons to swap which atom they orbit. This reasoning can be extended to say that the outer electrons of every atom in the solid can trade places implying that they all share one common energy state that extends throughout the entire crystal. As mentioned previously, the Pauli exclusion principle dictates that the electrons

must each be in a unique energy state. This requirement is satisfied if the electrons each occupy very slightly different energy levels. These similar but distinct energy levels can be thought of as a 'band' of available states made up of many closely spaced energy levels. This idea of bands made up of finite similar but unique states can be visualised in Figure 2.1.

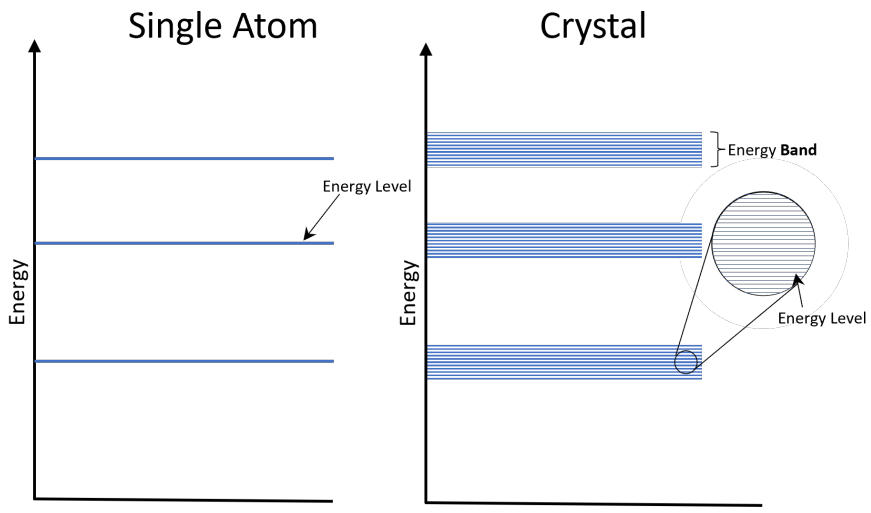

Figure 2.1: Visualization of available states for electrons in a single atom compared to a crystal.

The general electrical differences between semiconductors, insulators, and conductors can be explained by the degree to which their energy bands are filled. Electrons preferentially fill lower energy states and at low temperatures, will occupy the lowest existing energy levels. In a semiconductors, there are an even number of valence electrons resulting in the highest energy band being filled while the next level up is empty. This is similar for insulators though the energy gap between the filled and empty bands is larger in insulators. Conversely, at low temperatures, the outermost band in materials with an odd number of valence electrons such as aluminum is only half filled. Electrons within this half filled

band require very little additional energy to be promoted to one of many higher energy states within the same band. In conductors, a small applied electric field is able to excite electrons to higher energy states and allow current to flow. In both insulators and semiconductors, in order for electrons to be promoted, they required enough energy to jump to the next empty energy band. This energy difference between the highest occupied band and lowest unoccupied band is known as the materials bandgap.[15]

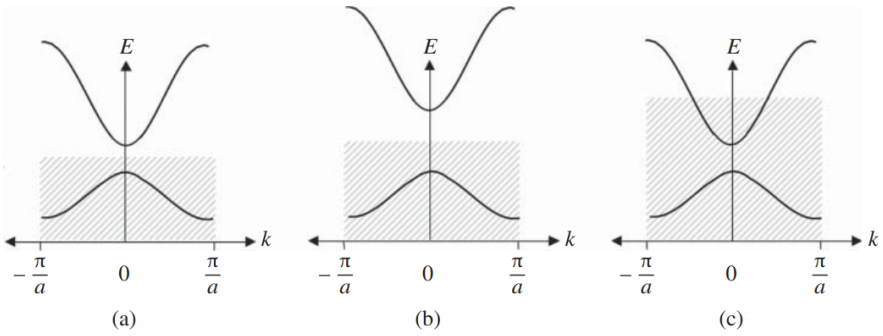

Figure 2.2: Filled electron states (shaded) in semiconductors, insulators, and metals and temperatures near absolute zero.[15]

At temperatures above absolute zero, some electrons will occupy higher states and it is not possible to know whether a specific energy state will be filled.

$$F(E) = \frac{1}{1 + \exp(\frac{E - E_f}{kT})} \tag{2.1}$$

The Fermi-Dirac distribution function, Equation 2.1, describes the probability of state with energy E being fill at a temperature of T where E_f if the Fermi energy and represents the energy of a state with a probability of being filled of $\frac{1}{2}$. Figure 2.3 shows the shape of this relation at several different temperatures. We can see that at sufficiently low temperatures, the lowest energy states will be

filled with 100% probability and that as temperature increases there is a chance that higher energy states will be occupied resulting in the distribution function changing from a step function to a continuous curve with decreasing slope.

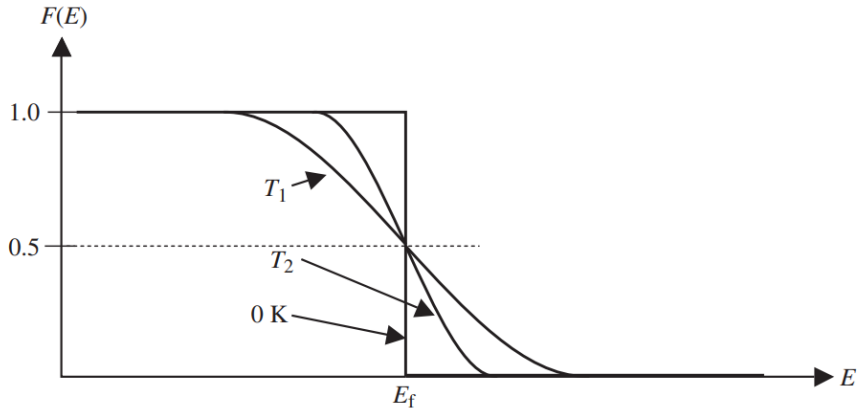

Figure 2.3: Fermi-Dirac distribution function at 0 K and two temperatures such that $0\,\mathrm{K} < T_2 < T_1$.[15]

2.2 Direct & Indirect Bandgaps

Semiconductors can have bandgaps that are either direct or indirect. That is to say, the energy maxima of the valence band and the energy minima of the conduction band can either be vertically aligned (Direct) or offset (Indirect). This configuration determines what conditions must be met for an electron to move from the valence to the conduction band. Electrons can gain energy by absorbing a photon (Optical excitation). The absorption of an electron can be seen on a band diagram as nearly perfect vertical movement. This is due to the fact that photons carry a very small amount of momentum (represented by movement along the horizontal axis) for their given energy. In a direct gap semiconductor, this means that photons with energy equal or greater to the bandgap (E_g) can be absorbed by valence electrons in order to jump to the conduction band. For an

indirect gap semiconductor, the absorption process is often not this simple. By absorbing a photon with energy equal to E_g, an electron would move up the band diagram but would not reach the conduction band as the conduction minima is offset from the valence maxima. In this case, the photon alone cannot excite the electron across the bandgap and instead a two-step absorption process must occur. In addition to the photon, a lattice vibration known as a phonon must also be present. Since phonons represent movement of lattice atoms, they carry significant momentum due to their mass when compared with electrons or photons. In a two-step absorption, the energy (vertical shift) required is largely provided by the photon while the phonon supplies the required momentum change (horizontal shift) for an electron to reach the bottom of the conduction band. Direct absorption in direct gap semiconductors for a range of photon energies is shown in Figure 2.4a. Figure 2.4b shows the two-step absorption process that occurs for photons near the gap energy as well as the possible direct transitions that can occur due to the absorption of photons with energy larger than the gap. Both the one-step and two-step absorption of photons can occur in reverse, resulting in the emission of a photon. The single step absorption or emission of a photon is generally orders of magnitude more likely to occur than the process that requires a phonon. This is very relevant to light emitting diode (LED)s as it explains why LEDs are almost exclusively fabricated from direct gap semiconductors, and by extension, why indirect gap materials exhibit such low emission efficiency.

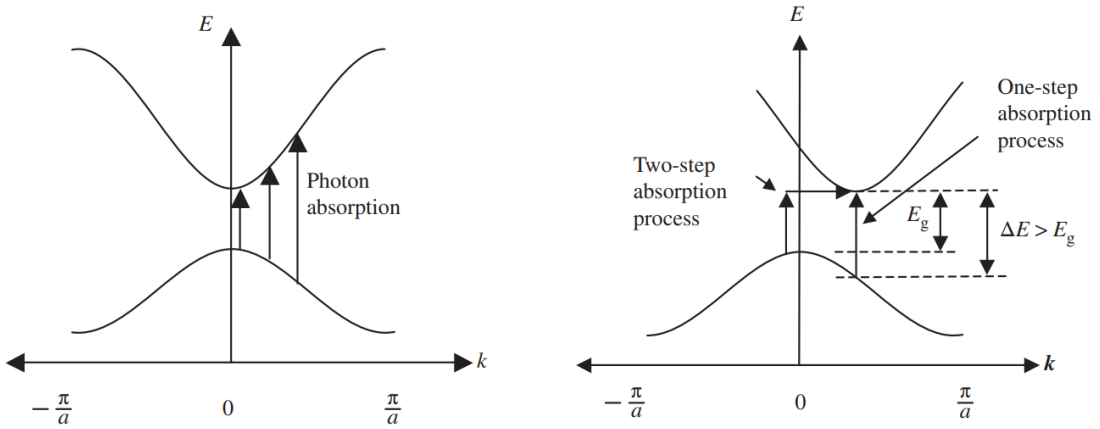

(a) Direct gap band diagram

(b) Indirect gap band diagram

Figure 2.4: (a) Promotion of an electron to the conduction band through direct absorption of photons with energy equal or greater than the bandgap (E_g). (b) Promotion of electron due to two-step phonon assisted absorption of photon with energy equal to bandgap E_g, and direct absorption of photons with energy greater than bandgap (E_g).[15]

2.3 P-N Junction

A P-N junction most basically consists of a p-type semiconductor joined with an n-type semiconductor resulting in a junction forming between the two regions. P-N junctions found wide scale use in simple logic circuits and as a rectifier due to their ability to allow current flow in one direction but block flow in the opposite direction.

A p-n junction in equilibrium (under no external bias) has four different currents flowing that cancel and result in a net zero flow of current across the junction. Minority carriers that enter the transition region will be subject to the built in electric field. This results in a drift current of electrons from the p-side to the n-side and of holes from the n-side to the p-side. At the same side, majority carriers will diffuse across the transition region due to the concentration gradient. These

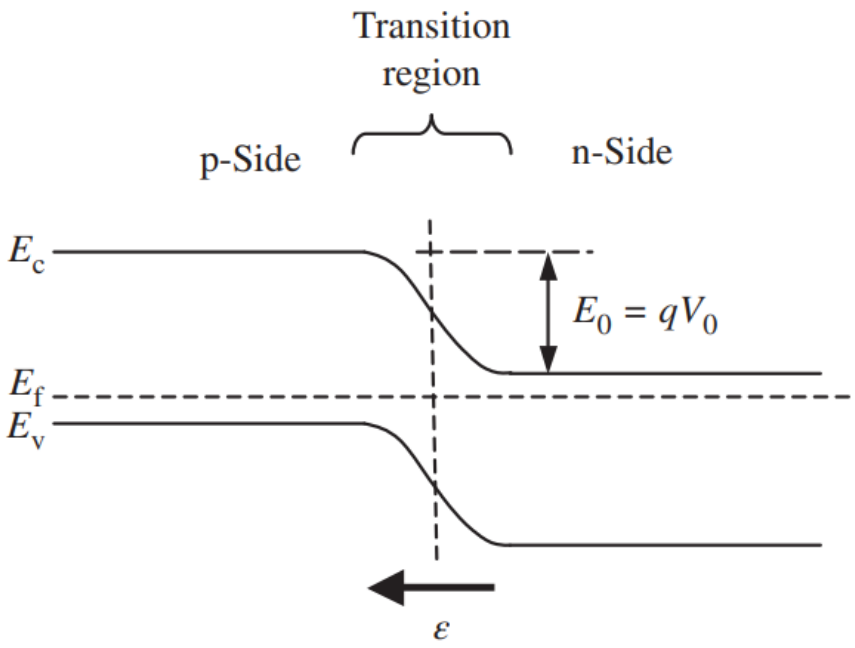

Figure 2.5: Band model of a basic p-n junction showing constant Fermi energy (E_f) and built in potential of the junction (V_0).[15]

two flows oppose each other, resulting in a net zero current flow on both sides of the junction.

When an external voltage is applied across the junction, these currents no longer sum to zero and there is net current flow through the junction. When a voltage is applied such that the p-side is connected to the positive terminal, the energy barrier and the electric field across the transition region will decrease as seen in Figure 2.6a. This results in lower drift currents which are not large enough to oppose the diffusion currents due to the majority carriers resulting in a a non zero current flowing. This junction is said to be operating in forward bias.

Conversely, applying a negative voltage across the junction will cause it to operate in reverse bias. In this case, the energy barrier and electric field will

increase as seen in Figure 2.6b. The resulting reverse current will be small as the drift current is limited by the number of minority carriers available to contribute to drift. Since the current is limited by the number of minority carriers, the net current is mostly independent of the applied voltage and quickly reaches a value known as the reverse saturation current, I_0.

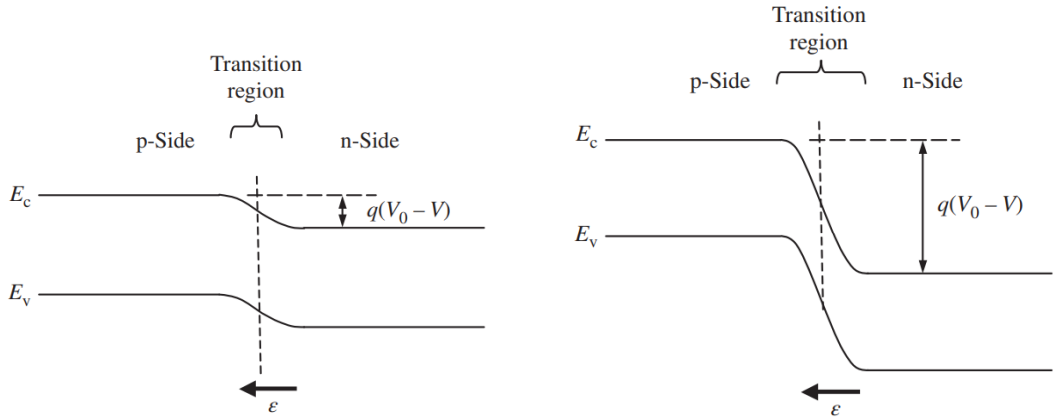

(a) Forward biased band model (b) Reverse biased band model

Figure 2.6: (a) Forward bias of a p-n junction showing a reduction of the energy barrier and electric field across the transition region. (b) Reverse bias of a p-n junction showing an increase in energy barrier and electric field across the transition area.[15]

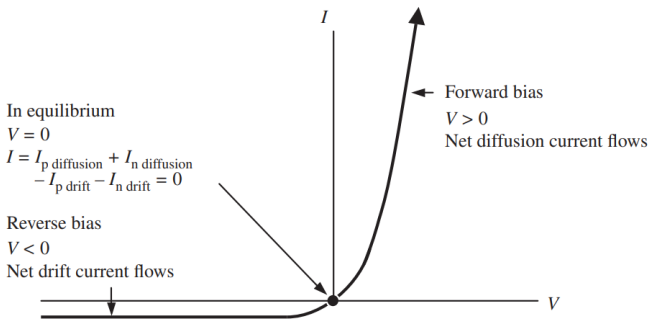

Figure 2.7: Plot of current-voltage curve of a p-n junction.[15]

It can be seen in Figure 2.7 that in forward bias, a small increase in applied voltage can result in a large increase in current flow, while in reverse bias, the

current saturates and remains constant. This illustrates how p-n junctions act as one-way valves, allowing current to flow in one direction but effectively blocking flow in the opposite direction.

2.4 LED Operation

In its most basic form, an LED is simply a p-n junction. In fact, all p-n junctions, including those used as rectifiers or logic components, will emit some light while under forward bias. Majority carriers are injected into the junction (electrons from n-side and holes from p-side) and recombine, releasing some energy. LEDs are designed to maximise the number of radiative recombinations while ensuring that emitted light can leave the device and not get reabsorbed.

Nonradiative recombination can occur through a variety of mechanisms involving lattice defects and carrier-carrier interactions, the specifics of these are detailed in section 2.6.

Since each instance of non-radiative recombination still takes energy, it results in a lower device efficiency. Because of this, great care is taken in both the design and fabrication of devices to minimize this phenomenon.

2.5 Phonons

The electrical, optical, and thermal behaviour of materials, particularly semiconductors, is often explained and more easily understood by utilising '*quasiparticles*'. Treating vacancies of electrons as a 'hole', a quasiparticle with positive charge, is a

prime example, but far from the only one. Phonons are quasiparticles that describe quantized lattice vibrations. These vibrations can interact with electrons and are particularly important as a source of momentum in indirect-gap semiconductors.

There are two types of phonons, acoustic and optical. Acoustic phonons describe longitudinal lattice vibrations with atoms moving in the same direction as each other much like sound waves through a material. Optical phonons arise when a unit cell of the lattice has two atoms in it. Optical phonons are vibrational modes in which the atoms in a unit cell move opposed to each other (illustrated in Figure 2.8). This out of phase oscillation creates a periodic dipole and allows optical phonons to couple with the electromagnetic waves of light. Optical phonons only appear in materials that have more than one atom per unit cell.

Acoustic phonons have frequencies in the gigahertz range while optical phonons tend to have much higher frequency in the terahertz range. This higher frequency also means that optical phonons have much more energy than acoustic.[16]

As mentioned in Figure 2.4, phonons are involved in the absorption and emission of light and are of particular significance in indirect-gap semiconductors.

In an indirect transition, a phonon can be either absorbed or emitted such that the following equation is satisfied:

$$h\nu = E_g \pm E_p \tag{2.2}$$

Where $h\nu$ is the photon energy, E_g is the energy gap between the initial and

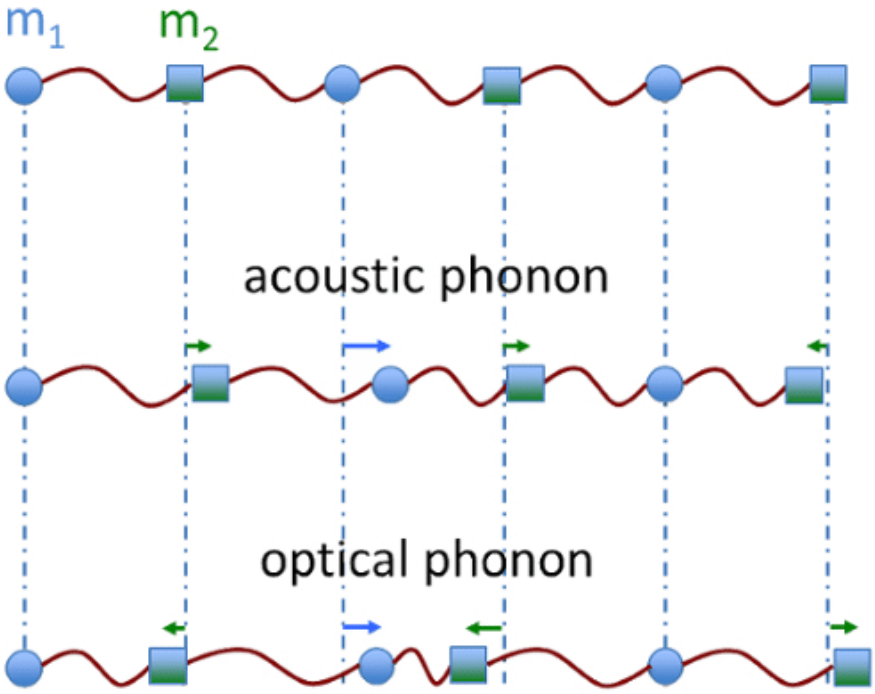

Figure 2.8: Phonons in a one dimensional chain of two different atoms with masses m_1 and m_2.[17] In acoustic phonons, adjacent masses generally move in the same direction (in-phase) while in optical phonons, adjacent masses oscillate out of phase.

final energy states $(E_i - E_f)$, and E_p is phonon energy with the sign denoting whether phonon absorption or emission occurs.

The absorption coefficient α is proportional to the probability of incident photons interacting with one or more phonons. The probability of phonon interaction is a function $f(N_p)$ of the number of phonons, N_p, with an energy of E_p.[18] Phonons are bosons so N_p is described by Bose-Einstein statistics:[18]

$$N_p = \frac{1}{\exp \frac{E_p}{kT} - 1} \tag{2.3}$$

This relation describes how an increase in temperature increases the concentration of phonons.

2.6 Nonradiative Recombination

Nonradiative recombination describes the recombination of EHPs that do not release a photon. This naming only suggests that a photon is not emitted and as such, a variety of mechanisms fall under this category.

Auger recombination is one such example. Auger recombination is a process often between two electrons and one hole (The opposite is also possible) where a second electron also in an excited state absorbs the energy from the electron hole recombination and is promoted further up into the conduction band. This energetic "hot" electron loses this energy through the release of multiple phonons and returns to the edge of the conduction band.[18] This process scales with charge carrier concentration squared.

Defects and impurities can also provide nonradiative pathways by creating a continuum of states between the two bands. Figure 2.9 shows a nonradiative center with radius, r. Charge carriers within a diffusion length, $\mathscr{L}$, will be attracted to this trap and recombine without releasing a photon. Recombinantion through the trap depicted in Figure 2.9 does not have a strong temperature dependence and can still occur at low temperatures.

Defects can also deform the bands around them as shown in Figure 2.9. These deformations act as barriers that must be overcome in order for the recombination to occur. In this case, there is a strong temperature dependence to recombination

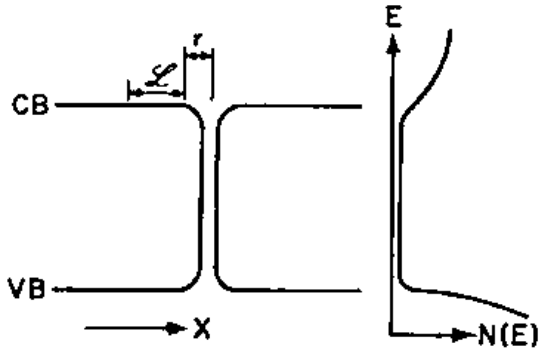

Figure 2.9: Continuum of states created by and localized to a defect or inclusion.[18]

as the charge carrier must have sufficient energy to overcome the barrier before it can recombine. At low temperatures, these traps will be largely inactive. [18]

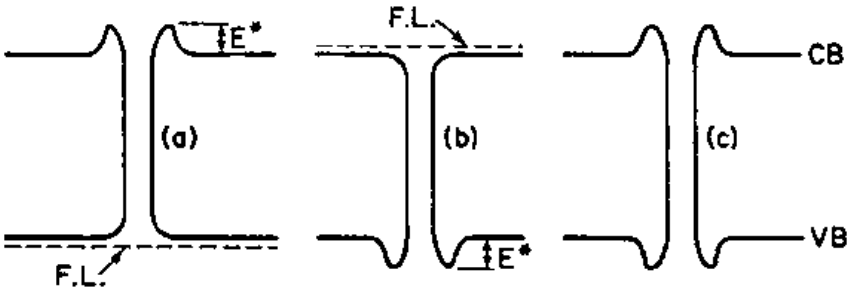

Figure 2.10: Nonradiative recombination centers surrounded by a barrier.[18]

2.7 Diffusion of Charge Carriers

Charge carriers are able to move throughout a material through diffusion. Diffusion of charge carriers is analogous to the diffusion of atoms in a solid. Atomic diffusion is driven by the random motion of atoms colliding in concentration gradient with the net result of movement from high concentration to low concentration. Diffusion of charge carriers is also driven by a concentration gradient. In this case it is a

concentration gradient of electrons, and there will be a net movement of electrons to an area with lower concentration. This is also true of holes. This motion can be written as

$$\Phi_n(x) = -D_n \frac{dn(x)}{dx} \tag{2.4a}$$

and

$$\Phi_p(x) = -D_p \frac{dp(x)}{dx} \tag{2.4b}$$

where $\Phi_n(x)$ and $\Phi_p(x)$ is the flux of electrons or holes respectively moving in the x direction. The negative sign indicates that the movement is from higher to lower concentration. A net flux of charge is an electric current and so Equations (2.4a) and (2.4b) can be rewritten as

$$J_n(x)_{diffusion} = qD_n \frac{dn(x)}{dx} \tag{2.5a}$$

$$J_p(x)_{diffusion} = -qD_p \frac{dp(x)}{dx} \tag{2.5b}$$

Note that in Equation (2.5a), the negative charge of the electron cancels with the negative denoting direction.

While diffusing, charge carriers are still subject to recombination and as such have an average distance they can travel before recombining. This is known as the diffusion length (L_n) and is governed by the diffusion coefficient (D_n) and carrier lifetime (τ_n).[15]

$$L_n = \sqrt{D_n \tau_n} \tag{2.6}$$

2.8 Silicon Carbide Polytypes

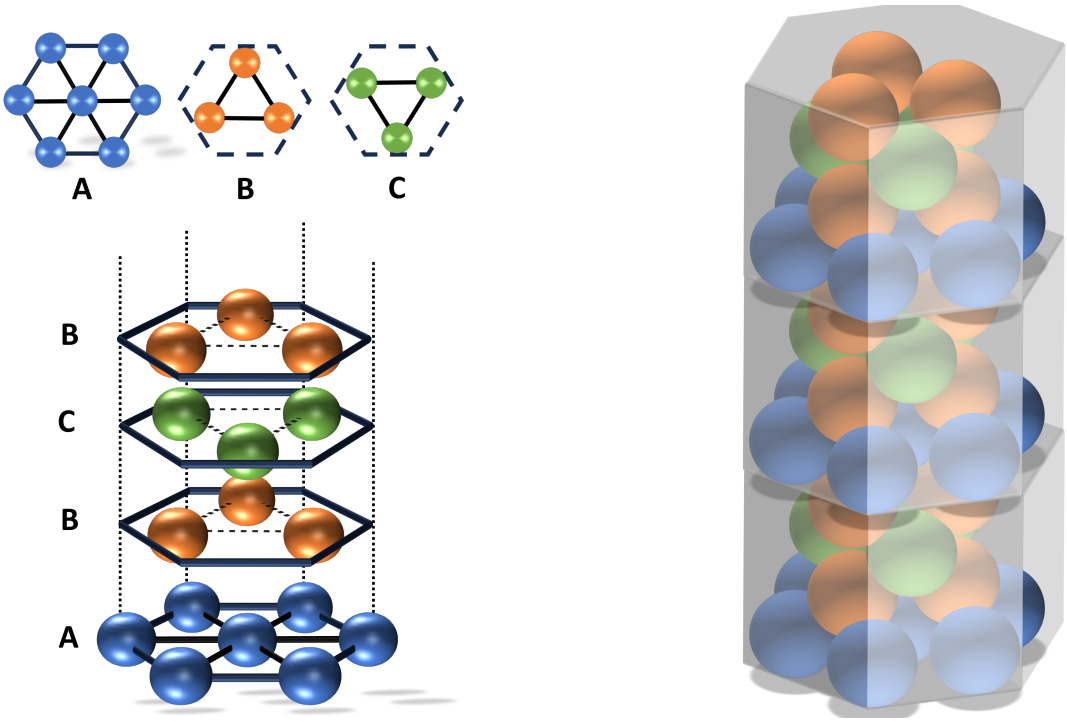

(a) Stacking pattern of 4H SiC. Possible orientations of bilayers noted as A, B, and C.

(b) Structure of 4H SiC showing repeating pattern after every fourth bilayer.

Figure 2.11: Possible orientations of silicon/carbon bilayers, and example of 4H stacking.

Silicon Carbide belongs to a group of materials that display polytypism. The crystal can take a number of different structures while still being described by the same chemical formula, reminiscent of how graphite and diamond are both pure carbon. In SiC, the crystal structure is made up of stuctural base units in the form of stacking bilayers (one silicon and one carbon). Each polytype is made up

of a different repeating pattern of these stacked bilayers which can be orientated in three ways, rotated 120 deg around the stacking axis.

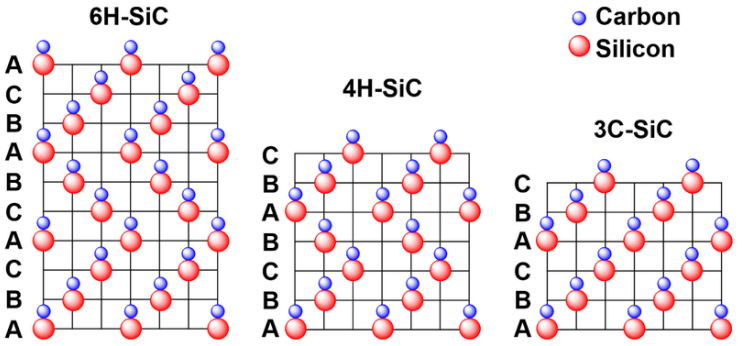

Figure 2.12: Stacking patterns of the most commonly used SiC polytypes (6H, 4H, 3C) [19]

There are over 100 different polytypes of silicon carbide each with unique material properties. The most commonly manufactured include 3C, 4H, and 6H-SiC, the stacking pattern and material properties of which are shown in Figure 2.12 and Table 2.1 respectively. The bandgap difference between 3C and 4H-SiC is 0.90 eV and corresponds to a emission difference of 145 nm from green (3C) to deep violet (4H)

2.9 Electrochemical Etch of Silicon Carbide

Silicon carbide boasts extreme chemical resistance alongside its impressive electrical properties. While good for the longevity and stability of devices, it poses a challenge when it comes to fabrication, as there are limited processes that are suitable for the patterning of silicon carbide. Simple wet etching is not possible as SiC is effectively universally resistant to acids, bases, solvents, and oxidizers as

Table 2.1: Material properties of common SiC polytypes at 300 K. From [20]

Property	**3C-SiC**	**4H-SiC**	**6H-SiC**
Bandgap E_g (eV)	2.36	3.26	3.02
Lattice constant (Å)	4.46	$a = 3.09$ $c = 10.08$	$a = 3.09$ $c = 15.12$
Relative permittivity	9.7	10	10
Hole mobility (cm^2/Vs)	40	120	90
Electron mobility (cm^2/Vs)	1000	$\parallel c$ axis: 1200 $\perp c$ axis: 1000	$\parallel c$ axis: 100 $\perp c$ axis: 450
Electron saturation velocity (10^7 cm s^{-1})	2.5	2	2
Thermal conductivity (W cm^{-1} K^{-1})	3-5	3-5	3-5

shown in Figure 2.13. Reactive-ion etching (reactive ion etching (RIE)) is suitable for removing material and is used in industry for creating features for devices including deep etches and mesas.

Variations in wet etching, however, can considerably alter the surface and and underlying bulk material. Electrochemical and photo-electrochemical etching are examples of processes that can create a layer of porous SiC with an extremely wide range of morphologies. The resulting structures are effected by parameters such as voltage, chemistry of electrolyte, illumination intensity/wavelength, and orientation of wafer (what face is being etched).

Figure 2.14 shows the pores formed by an electrochemical anodic etch using two different concentrations of HF. Figure 2.14a has a wall thickness of 30 to 200 nm skewed towards thicker walls while the higher concentration etch (Figure 2.14b) shows more uniform formation of pores with an average diameter of 150 nm and a wall thickness of 20 to 30 nm. [22] Figure 2.15 shows samples etched in a

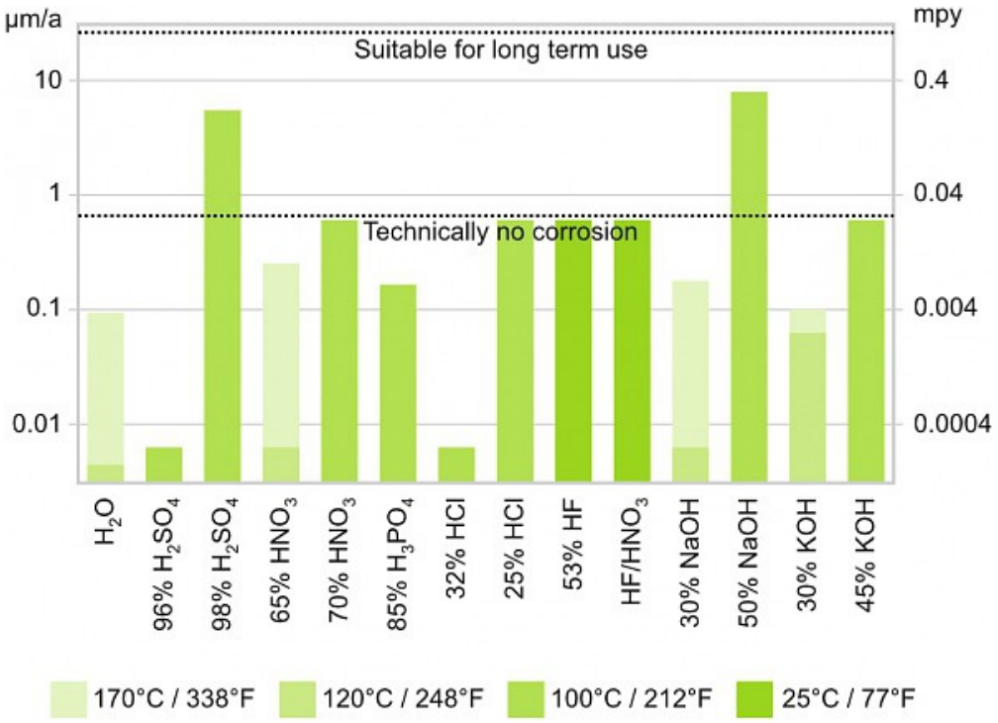

Figure 2.13: Corrosion rate of Pressureless sintered silicon carbide in micrometers per year (µm/a) and milli-inches per year (mpy). From [21]

similar chemistry (HF) with the addition of an HgXe arc lamp providing a flux of ultraviolet (UV) photons with an intensity of 600 mW/cm^2. The variation in columnar pore growth is attributed to the difference in the oxidisation rate of different crystal faces, where Si-face < a-face < C-face. [23]

The electrochemical reaction can be broken into two distinct steps. First, the SiC reacts with water and holes (h^+) from the applied voltage and incident UV photons to create SiO_2 and release CO and CO_2 as a gas (Equations (2.7) and (2.8)). The second part of the reaction involves the HF removing the newly formed SiO_2 in order to expose new SiC to be oxidised, at which point the reaction cycle can repeat.[23]

$$\mathrm{SiC} + 3\,\mathrm{H_2O} + 6\,\mathrm{h^+} \longrightarrow \mathrm{SiO_2} + \mathrm{CO} + 6\,\mathrm{H^+} \tag{2.7}$$

$$\mathrm{SiC} + 4\,\mathrm{H_2O} + 8\,\mathrm{h^+} \longrightarrow \mathrm{SiO_2} + \mathrm{CO_2} + 8\,\mathrm{H^+} \tag{2.8}$$

$$6\,\mathrm{HF} + \mathrm{SiO_2} \longrightarrow \mathrm{H_2SiF_6} + 2\,\mathrm{H_2O} \tag{2.9}$$

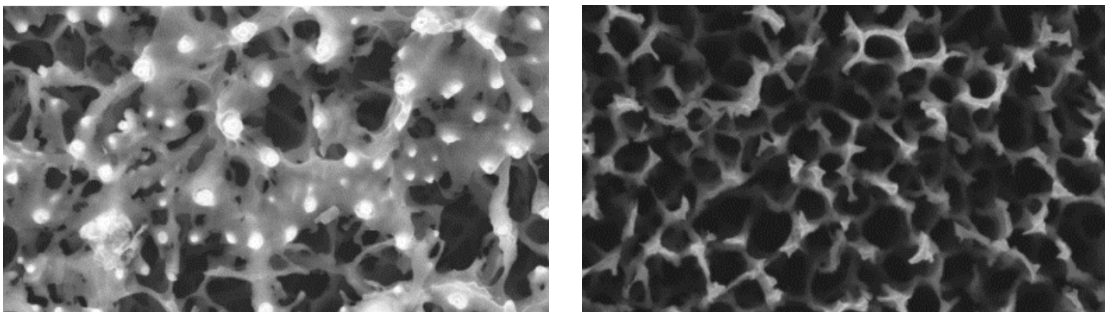

(a) 10% HF - 5% Ethanol (b) 20% HF - 5% Ethanol

Figure 2.14: Porous silicon carbide fabricated through electrochemical etching at 20 V. The sample pictured in b) had a dense low porosity top layer that was removed with RIE (90% SF_6 and O_2) to reveal uniform porosity.[22]

By tuning etch parameters, a wide range of surface morphologies is achievable.

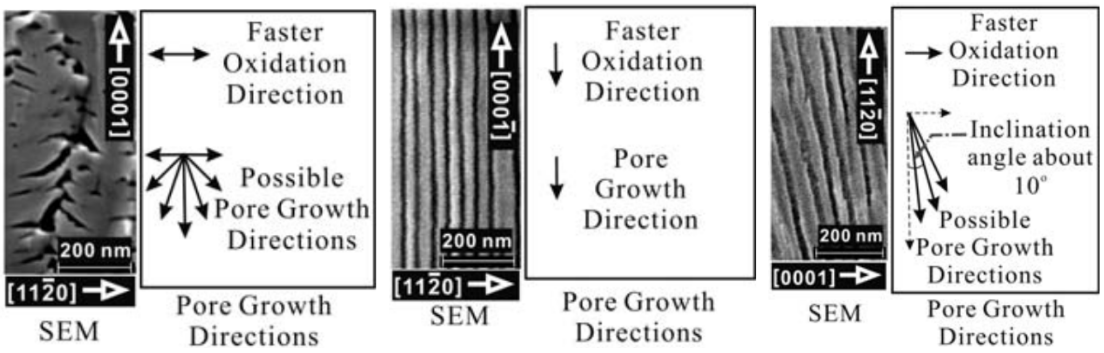

(a) Si-face (b) C-face (c) a-face

Figure 2.15: Comparison of pore growth between different etched faces on 6H silicon carbide. a) Growth of pores on the silicon face is disordered and dendritic due to lateral oxidation preference. b) Etching the carbon face of the crystal results in vertical self-ordered columnar nanopores due to the favoured oxidation direction being aligned with the direction of electric field. c) Etching of the a-face results in columnar nanopores skewed to the side where oxidation occurs faster. The resulting pores are not as uniform when compared to the carbon face, as there is a range of angles over which the pores can propagate.[23]

Chapter 3

Experimental Methods

3.1 Sample Preparation

Devices for commercial use are generally fully packaged for through hole or surface mounting. This plastic packaging needs to be removed in order to expose the bare die both for observation and reverse engineering.

The following details the general processes used to prepare samples prior to experimental work. Any specific deviation from this process will be highlighted in the relevant chapter. The specific commercial device used was the GeneSiC GA0JT12-263 as pictured in Figure 3.1.

3.1.1 Decapsulation

Decapsulation or decapping is the process of removing the protective packaging in order to expose the surface of the Die in order to allow visual inspection or electrical probing of the integrated circuit (IC). This is often done in order to trouble shoot

Figure 3.1: Close up image of the GeneSIC GA05JT12-263 T31325 used for experiments Prior to any decapsulation.

manufacturing errors, ensure authenticity of chips, or to aid in reverse engineering of a device.

Decapsulation of polymer packages is often done using a combination of physical milling to reduce excess plastic followed by an etch step using either hot concentrated acid (Sulfuric or Nitric) or a plasma (Primarily oxygen). The most simple method involves first selectively milling excess plastic above the area to be exposed. The device is then placed in a dish to catch excess acid and then heated on a hotplate. Once the temperature reaches 100 C, a pipette is used to place a few drops of concentrated acid onto the milled part of the device package. The acid reacts with the polymer and additional acid is added as the reaction slows. This

is repeated until the section of interest on the die is exposed. The device can then be rinsed with acetone or isopropyl alcohol. [24]

This acid decapsulation method described above was attempted using concentrated sulfuric acid with limited success. This method is best used to expose the top surface of the die while use on the sides or back of the devices exposes the metal pins to the acid which react much more rapidly than the polymer and damages functionality. Furthermore, exposing the top of the die does not allow for adequate viewing of the active region without also removing the electrical contacts on the surface. For these reasons, a primarily mechanical decapsulation method was adopted with limited use of acetone to soften polymer remains and clean exposed regions. In addition, the avoidance of hot concentrated acid limits removes the risk of damage and corrosion to the metal pins allowing them to still be used to make electrical connection after processing.

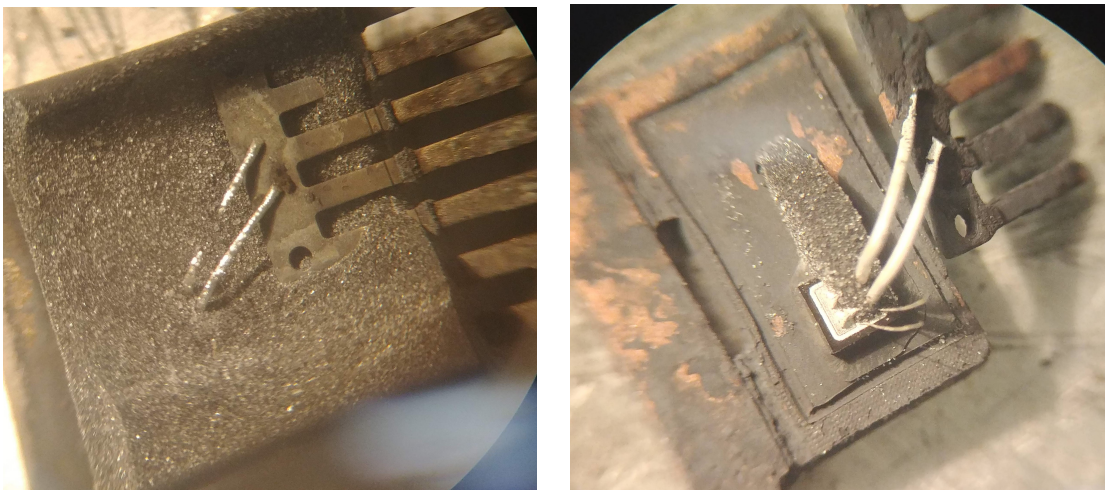

(a) (b)

Figure 3.2: Image of device internals after (a) some and (b) most of the polymer package was removed using the acid decapsulation method.

3.1.2 Exposing Die Side Edge

The device package was secured in a vice and an electric rotary tool with a diamond cutting wheel attachment was used to remove the side of the package until part of the die just barely became visible. The remaining layer of plastic was thin enough to scrape/peel away after being softened by exposure to room temperature acetone. The extreme hardness of silicon carbide allowed for manual removal in this way with limited risk of surface damage.

3.1.3 Cutting into Die Side Edge

The same rotary tool and diamond cutting wheel was used to grind a shallow amount into the side of the die in order to expose the active region (Junction) for processing.

3.1.4 Exposing Back Surface

The electrical connections needed to run the junction in forward bias are interdigitated and both located on the top surface of device leaving the back contact/surface unused during operation. This made the back surface of the die attractive as a potential 'viewing window' to observe the active region during operation.

Two methods were used to prepare these samples. First, wires were soldered to the pins of the package that correspond to the interdigitated contacts. The device was then submerged in a two part epoxy and placed in an oven overnight to harden. The resulting puck Figure 3.3 allowed for the sample to be more easily manipulated during grinding and testing.

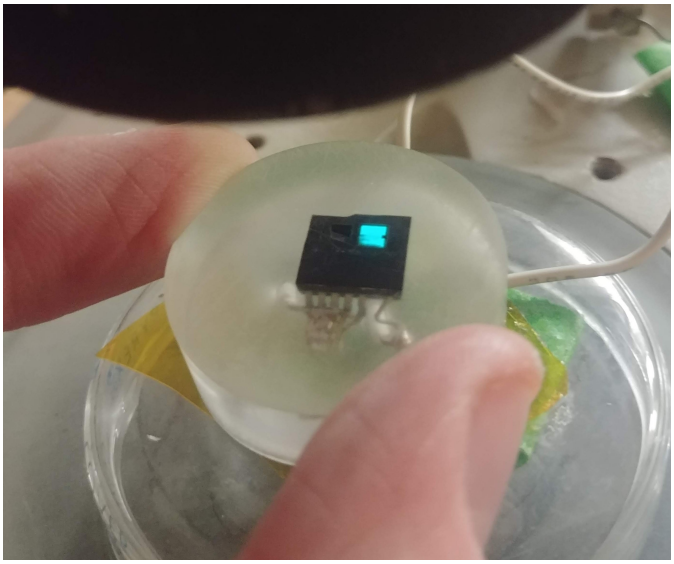

Figure 3.3: Sample embedded in two part epoxy resin.

The second method was adopted to prepare multiple samples simultaneously. To do this, four devices were fixed to the surface of an aluminum block with the back side facing up using heat activated mounting adhesive (Crystalbond) as shown in Figure 3.4. The four devices could then be simultaneously ground on an abrasive diamond wheel until the back surface of the die was reached and partially ground into. Care was taken to avoid grinding deep enough to reach the active region which would destroy the device. The rough ground samples were then polished using a series of diamond abrasive pastes (Up to 2 um) until the surface was visibly smooth without scratches and optically reflective.

After the samples were polished, the aluminum block was heated on a hotplate to melt the adhesive and allow the devices to be removed. Samples were subsequently immersed in isopropyl alcohol to remove any remaining adhesive and clean off any abrasives/debris from polishing.

(a) (b) (c)

Figure 3.4: Four samples mounted for grinding. (a) Mounted without grinding, (b) majority of back electrode and package removed, (c) Bare die surface exposed, ready for polishing and removal.

3.1.5 Bare-die Soldering

Prior to settling on packaged devices, attempts were made to use bare unpackaged dies. The contacts located on the top surface of the die (Source/gate) are aluminum and should be electrically connected using a wire bonding tool. Due to the tool being out of service attempts were made to solder directly onto the top pads. To avoid shorting, a thin piece of Kapton tape was used to mask off the area between the source and gate contacts. A solder paste formulated for soldering to aluminum was then placed on the pads with fine wires. The die was heated until the solder flowed and beaded into separate connections for the source and gate. The resulting connection was both electrically and mechanically poor as the solder did not wet the contact pads. It is likely that the solder/flux is not usable on such thin layers of aluminum. The process and poor results are shown in Figure 3.5. After multiple attempts, the decision was made to utilize packaged devices with the die already bonded to pins that can be soldered. This put limitations on what processes the sample could be put through as conditions needed to be suitable for the polymer

packaging and exposed pins.

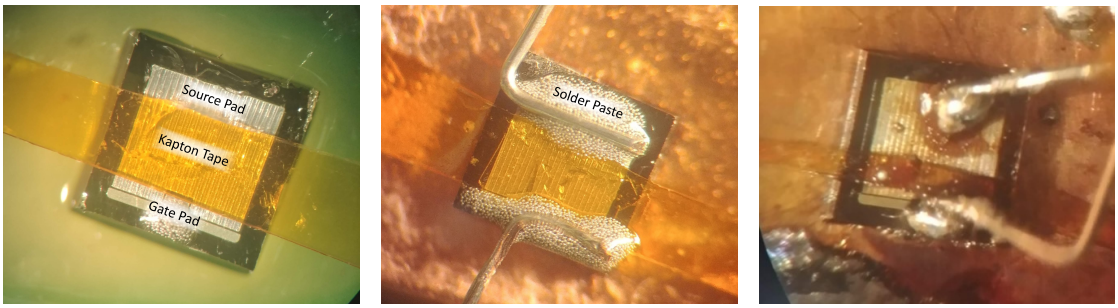

(a) (b) (c)

Figure 3.5: Adding electrical contacts to bare die. (a) Kapton tape applied as psuedo mask, (b) solder paste applied to contacts along with wires, (c) resulting beads of solder do not wet the pads.

3.2 Emission Spectrum Measurement

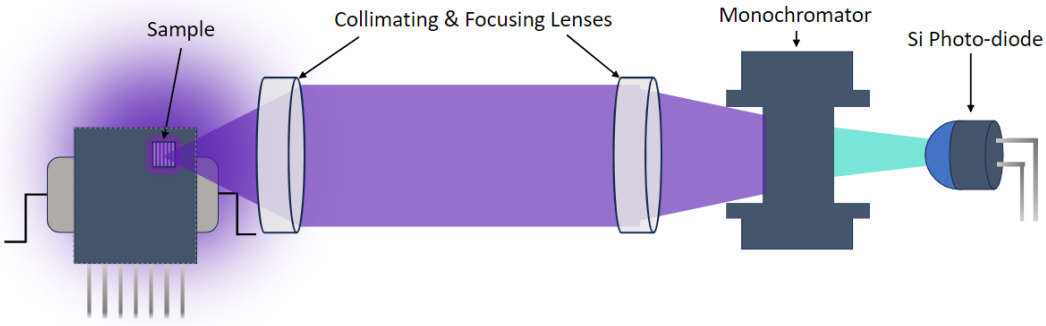

Figure 3.6: Schematic of experimental setup used to measure the emission spectrum of devices. Not to scale.

The sample was connected to a benchtop power supply and run in forward bias. Generated light was coupled into a series of lenses in order to collimate it. The collimated light was passed through a monochromator and was then incident on an avalanche photodiode. The resulting current of the diode is proportional to the

intensity of light emission (after accounting for response curve). The spectrum of light was captured by stepping through the relevant wavelength range using the monochromator and recording the current of the photodiode on a digital multimeter. The resulting spectrum was then divided by the response curve of the photodiode to obtain the true relative optical spectrum.

Chapter 4

Electroluminescence in SiC due to Lateral Charge Diffusion

4.1 Purpose

The concept of bipolar charge diffusion light emitting diode (LED)s involves and electrically active region where charge carriers are injected similarly to a traditional LED. The charge carriers then undergo diffusion into a second material where they undergo radiative recombination. The second material can be a entirely separate material (a direct gap material on the sides of an indirect one), or can be the same material with defects added or structures grown in order to allow for recombination to occur. LED devices based on lateral charge diffusion, also known as diffusion-driven charge transport (DDCT), have been demonstrated in GaInP/GaN and GaN. **\ac {ddct}**, [25]

Our work aims to demonstrate a silicon carbide diode with porous side walls

where bulk silicon carbide acts as the electrically active layer with poor recombination efficiency but allows for diffusion to the sidewalls of the device. The porous sides enhance recombination of carriers that diffuse from the bulk material by providing a high concentration of surface defects. Comparison of the emission spectrum of the device before and after etching (creation of porous region) will highlight effects of diffusion into the porous region.

4.2 Experiment

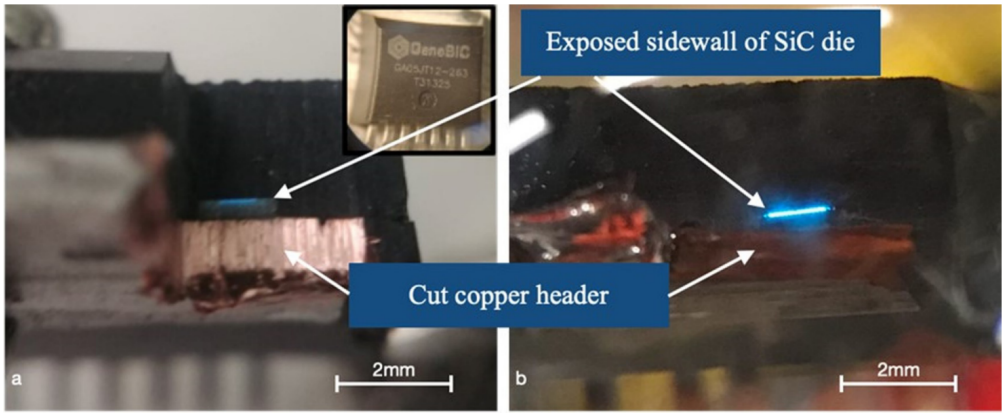

Figure 4.1: Exposed die of 4H-SiC GeneSiC GA05JT12-263 under forward bias. Inset image shoes device package, Left image shows a die sidewall that has been ground into. Right image shows an undamaged sidewall where package residue was removed chemically using acetone.

The devices used were 4H-SiC GeneSiC GA05JT12-263 with one side of the package ground down to reveal the bare die. Figure 4.1 shows two devices with the side of the die exposed while forward biased. The apparent difference in brightness can be attributed to the out-coupling of light through the rough cut edge or the smooth uncut surface. The emission spectrum of both types of device were measured according to section 3.2 before undergoing an electrochemical anodic

etch in HF as described below. After being etched, the spectrum was once again recorded to allow for comparison.

4.2.1 Etch Parameters

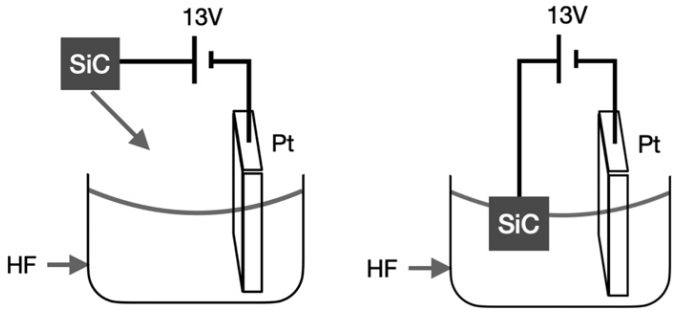

Figure 4.2: Schematic of electrochemical etch, from [20].

A solution of 20% hydrofluoric acid and 5% ethanol was prepared with distilled water in a Polytetrafluoroethylene (PTFE) beaker. The SiC sample was attached to the positive terminal (anode) of a benchtop power supply while a platinum electrode (Wire) was connected to the negative terminal (cathode). All electrodes of the device were connected to ensure even voltage across the device. Both the electrode and the sample were suspended in the solution such that the surface undergoing reaction would not be blocked by any generated gas. The electrochemical etch was run at 13 V for a duration of 4 minutes.

4.2.2 Sample Description

Sample i) had the package opened to expose the die sidewall but care was taken not to cut into the die. The spectrum can be seen in Figure 4.4a and shows two characteristic emission peaks. The sharp peak at 390 nm is attributed to phonon-assisted band-to-band transitions and free-to-bound transitions. The second broad

peak in the green region is due to a variety of lattice defects including stacking faults and dislocations. The spectrum for sample i) is largely unchanged after etching.

Sample ii) was prepared and etched similarly to sample i) with the key difference that the die was cut into while opening the package. Figure 4.5 shows how deep the die was cut and the spectrum before and after etching is compared in Figure 4.4b. Unlike sample i) the emission changes significantly after etching, with the green peak increasing relative to the 390 nm peak. It is important to note that each curve is normalized to itself and so conclusions about overall light emission cannot be made. This is done due to the etching process having an effect on the out-coupling of the light from the die surface.

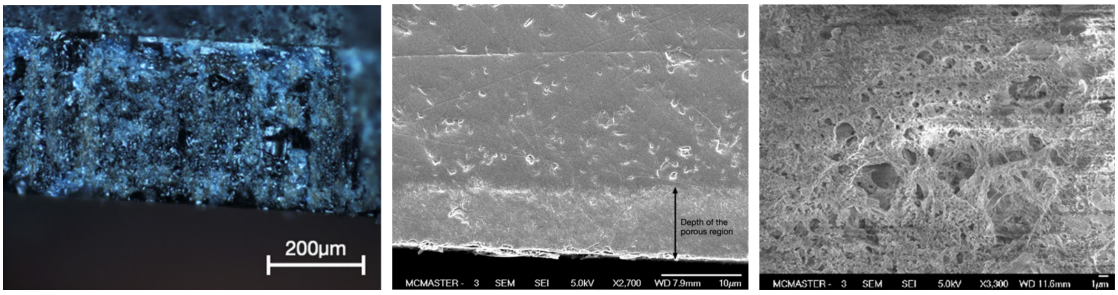

(a) Optical micrograph of surface after etch.

(b) cross-sectional SEM showing the depth of the porous layer.

(c) Higher magnification SEM of the porous surface layer.

Figure 4.3

Sample iii) (Figure 4.6) had the same emission peaks seen in previous samples with a small increase in the green peak after etching. For sample iv), strong peaks at 450 nm and 505 nm were observed (Figure 4.7), both of which disappeared post etch leaving a wide green emission similar to that of previous samples. The spectrum of sample v) showed a strong peak at 420 nm not seen in other samples

Table 4.1: Summary of samples tested. Dominant recombination methods are based off of emission peaks reported in literature. [20]

Sample	**Treatment**		**Ideality Factor**	**Dominant Recombination Method(s)**
i)	Cut	Pre-Etch Etched	...	Near-band-edge recombination Dislocations/stacking faults
ii)	Uncut	Pre-Etch Etched	...	Near-band-edge recombination Dislocations/stacking faults, carbon-related defects
iii)	Cut	Pre-Etch Etched	1.320 1.390	Near-band-edge recombination Dislocations/stacking faults, carbon-related defects
iv)	Cut	Pre-Etch Etched	1.266 1.346	Near-band-edge recombination Near-surface photoluminescent defects assumed
v)	Uncut	Pre-Etch Etched	4.373 4.711	Stacking faults ...

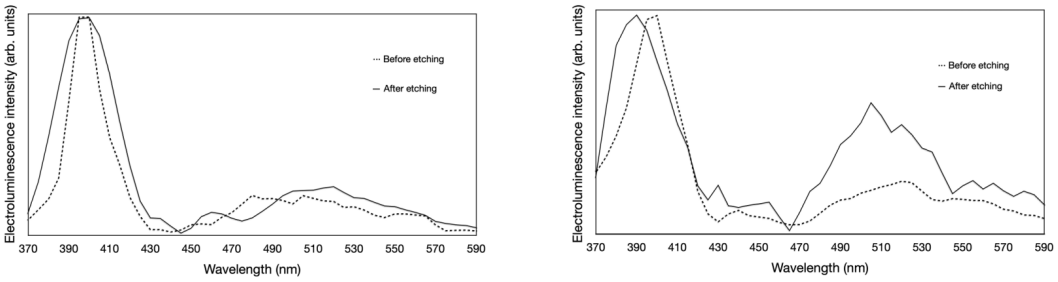

(a) (b)

Figure 4.4: Spectrum of (a) sample i) and (b) sample ii) before and after etching. Curves are self normalized and units are arbitrary. [20]

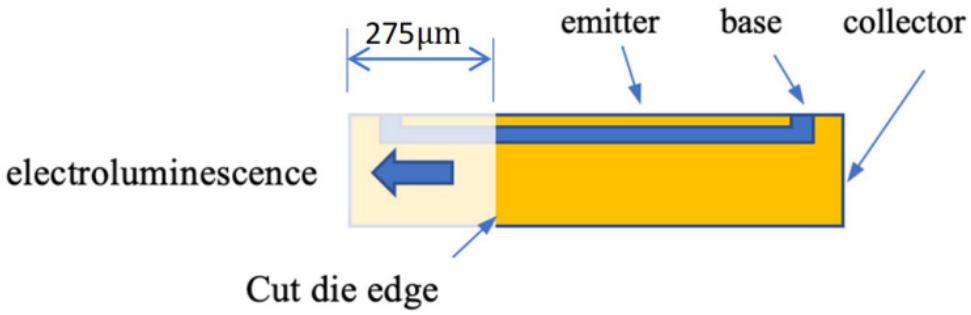

Figure 4.5: Schematic of sample ii) showing the depth to which the die was cut (275 µm). [20]

as well as little evidence of the typical 390 nm band-to-band emission. The ideality factors of sample v) which can be seen in Table 4.1 are significantly larger that those measured for other devices.

4.3 Discussion

The lack of spectrum change in sample i) suggests that the carriers are not able to diffuse far enough to reach the porous region. This makes sense as the porous region is outside of the guard ring present in on the die (Used to prevent breakdown at high voltages) and by extension far away from the flow of carriers. After cutting

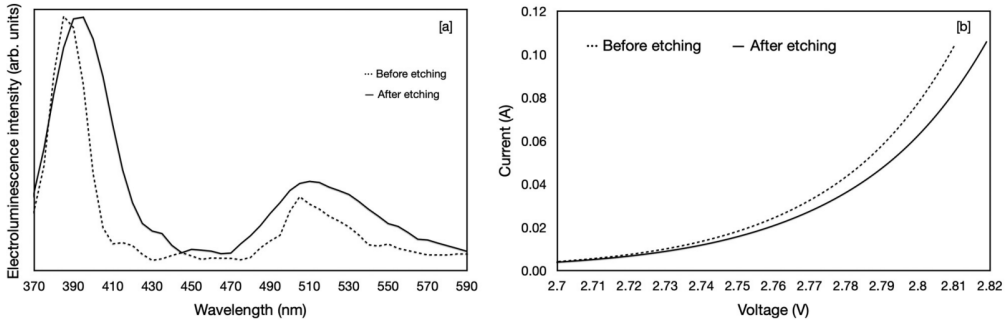

Figure 4.6: a) spectrum and b) IV curve of sample iii) both before and after etching. [20]

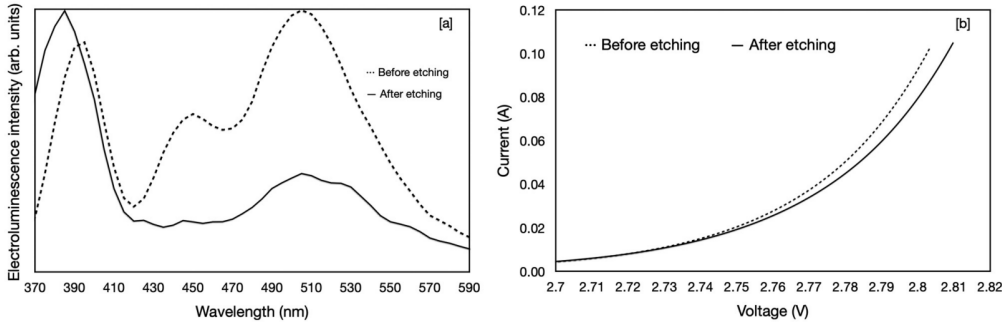

Figure 4.7: a) spectrum and b) IV curve of sample iv) both before and after etching.[20]

into the die in sample ii), the porous region is within the guard ring and much closer to the majority of carriers. The increase of the green peak in relation to the shorter wavelength peak seen in Figure 4.4b is a result of carriers diffusing into the porous layer and recombining at carbon related surface defects. Sample iii) also follows this trend though the increase in green emission is less dramatic.

The two peaks unique to sample iv) disappear after etching. This would be explained if they were due to defects with a depth limited to 10 µm which is approximately the depth that the etch step penetrates to as seen in Figure 4.3b. We would not however, expect any carriers to be reaching that far past the guard ring suggesting that these emission peaks are a result of photoluminescence rather

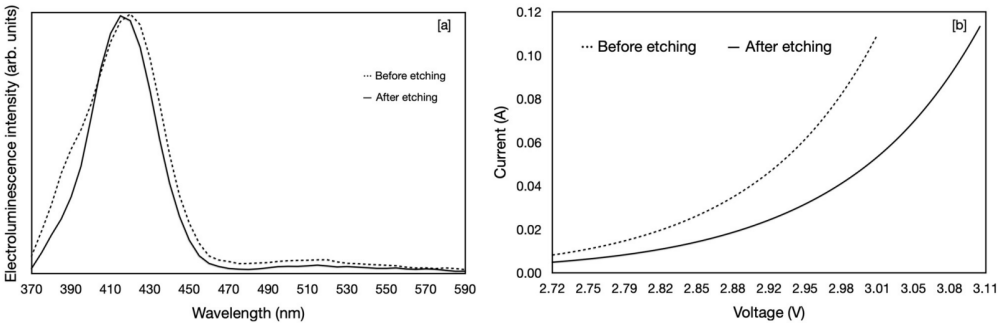

Figure 4.8: a) spectrum and b) IV curve of sample v) both before and after etching.[20]

than direct carrier recombination.

The emission spectrum of sample v) is dominated by a peak not present in any of the other samples measured. This peak at 420 nm is consistent with luminescence in SiC due to Shockley stacking faults or intrinsic Frank stacking faults reported in literature.[27] These defects can be formed during most fabrication steps including growth, oxidation, annealing and implantation or can appear in P-I-N diodes due to electrical stress. Etching with HF did not result in a significant change in emission suggesting that carriers were not able to reach the porous region as in sample i) and that the stacking faults responsible for the peak at 420 nm were not located near the etched surface.

The relative increase of green emission in samples ii) and iii) are understood as follows. Under forward bias, injected electrons and holes will diffuse laterally towards side walls due to a concentration gradient. After the samples were cut and etched, a layer of nanoporous silicon carbide is formed on the sidewall. This porous region is close enough to the junction that some charge carriers diffuse into it and are able to recombine radiatively due to the large surface and carbon related

surface states present. The concentration gradient causing the lateral diffusion is maintained by the constant injection of carriers resulting in the continuous radiative recombination within the porous region.

This lateral diffusion of charge carriers to an area spatially separate from the junction and subsequent recombination is similar to a mechanism reported in GaN and GaInP/GaAs devices. [25][25] A primary difference between reported examples of DDCT and our device is that our device is composed of an indirect bandgap semiconductor while other devices utilized direct gap materials.

This mechanism was only observed in samples where the die was cut prior to etching. This suggests that without the die being cut, the porous layer remained too far away from the active junction for carriers to reach it by diffusion. The diffusion length of holes in 4H-SiC varies according to preparation and growth methods but has been reported to be in the range of tens of microns.[20] With this diffusion length, the fraction of injected carriers that are able to reach the porous region is quite small even in the cut die samples as the full die has a width of 1 mm. Taking this into consideration, a device with a much smaller junction area such that all carriers could potentially diffuse to the sidewalls, and with a porous region on all sides would show a much more drastic increase in green emission.

4.4 Conclusion

We have demonstrated the concept of electroluminescence in nanoporous SiC due to bipolar lateral diffusion for the first time. Bipolar diffusion is presented as a mechanism to achieve radiative recombination using an indirect gap P-I-N diode.

A silicon carbide homojunction as the electrically active junction is demonstrated with nanoporous sidewalls as a recombination pathway. The underlying concept however, is appplicable to a broad range of materials and recombination pathways. Key concepts include:

- The electrically active region of the device can be made of an indirect gap semiconductor
- The recombination material can be formed, grown or deposited on the sides of the junction
- The material or pathway used for recombination can be changed without the need to change the electrically active region of the LED. Recombination pathways can be changed or included together to achieve desired wavelength emission
- Lateral diffusion driven charge transport is applicable to both homojunctions as demonstrated and heterojunctions.

Chapter 5

Reversible Heat Induced Blueshift in SiC P-I-N Diode

The purpose of the experiment is to characterize and suggest a mechanism for the observed blue shift that occurs at increased temperatures in a forward biased SiC P-I-N diode.

5.1 Measurement

The SiC device used was the same as in chapter 4. The preparation is described in subsection 3.1.4. After the back surface was exposed, a small hole was drilled in the side of the package and a thermocouple was inserted to measure temperature as close to the junction as possible. A power resistor was secured to the front of the package with thermal paste as an interface in order to allow for temperature adjustment independent of forward current driving the diode. Figure 5.1 shows how the thermal couple and resistor were positioned.

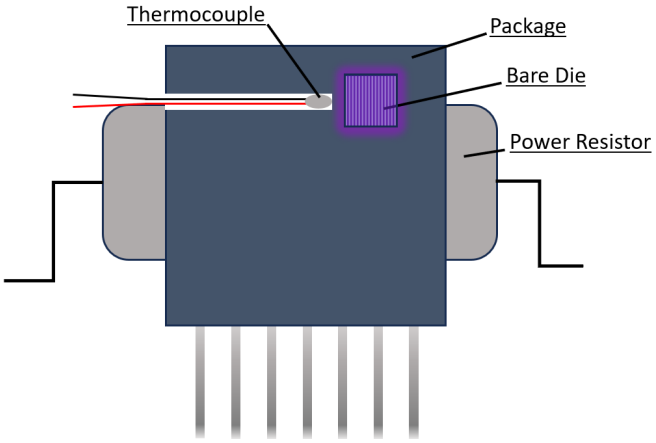

Figure 5.1: Diagram showing how thermocouple and resistor are oriented in relation to the device.

A spectrum of the sample was first taken with no additional heating (only heat due to forward bias). Subsequently, current was passed through the power resistor to raise the temperature measured by the thermocouple to 183 °C. The temperature chosen was arbitrary but was near the specified maximum temperature of the device (175 °C) and caused a visible colour change in emission.

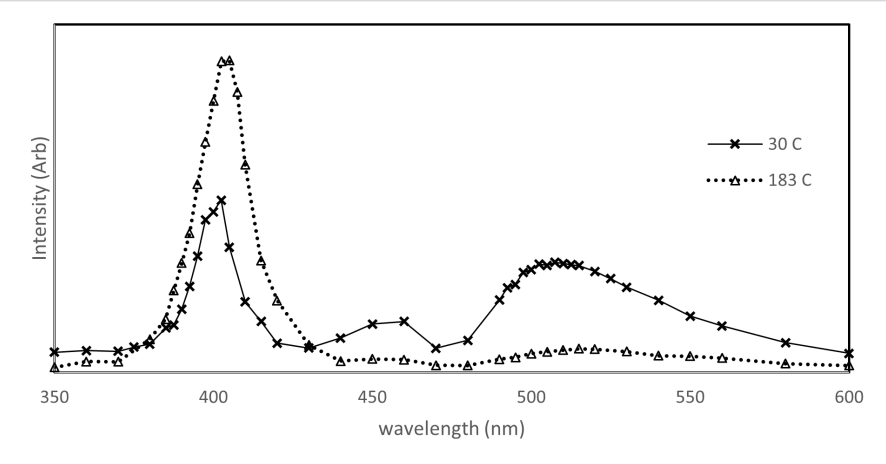

Figure 5.2: Emission spectrum of device with no additional heating (30 °C) and heated to 183 °C. The spectrum is corrected for the response curve of the photodiode. Intensity units are arbitrary.

The spectrum at each temperature can be seen in Figure 5.2. The 30 °C curve shows a sharp peak at 405 nm and an asymmetric broad peak centered around 510 nm with a long tail on the red side of the spectrum. The curve at 183 °C shares the general shape but the first peak at 405 nm is drastically increased and the green peak, while still present, is greatly suppressed. There is also a small peak present at 460 nm that effectively disappears when the heat is applied.

5.2 Discussion

5.2.1 405 Nanometer Peak

The broad green peak observed is similar to the one discussed in chapter 4 and is attributed to a number of different lattice defects including stacking faults and dislocations. When heated, this peak is suppressed but still remains.There is no discernible peak at 420 nm from single Shockley stacking faults as observed in sample 5 in chapter 4. The first peak resembles the 390 nm peak known to be a result of phonon assisted band-to-band transitions that was also observed in chapter 4. However, the peak is shifted and centered around 405 nm. This wavelength does not match any emission mechanisms or defects reported in literature. One paper was found that observed a peak shift from 390 nm to 405 nm after being passed through a 400 µm substrate of 4H-SiC and epi-layers of 6H-SiC. This was attributed to the greater absorption of higher energy photons near the bandgap leading to the red-shift observed in the first emission peak.[28] This could contribute to the observed shift from the peak measured in chapter 4 as the light travels a different path to exit the device as illustrated in Figure 5.3. Specifically, all light exiting the

sample through the bottom-face passes through he entire thickness of the substrate and is subject to the preferential absorption of higher energy photons.

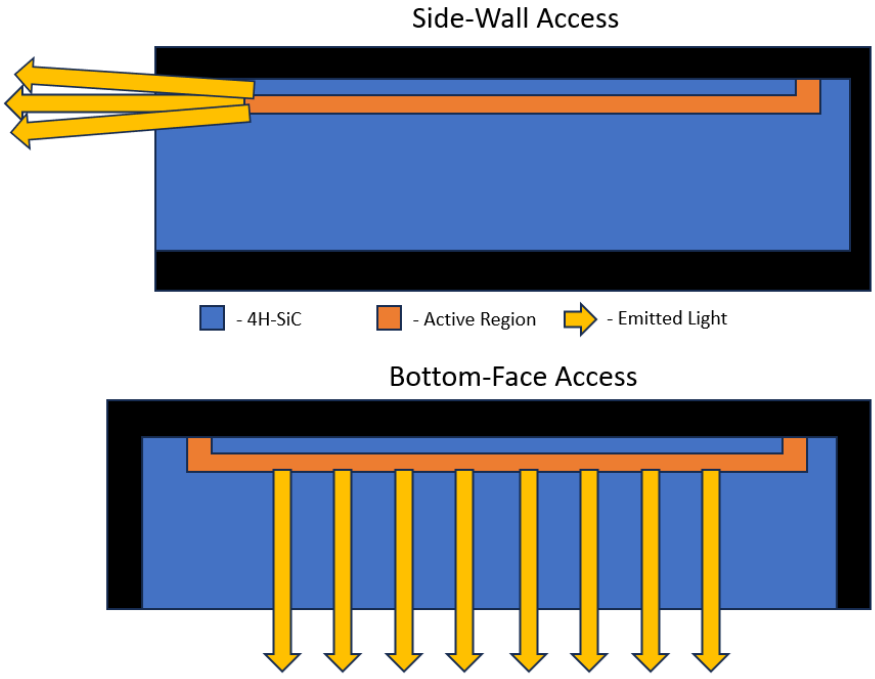

Figure 5.3: Comparison of samples used in chapter 4 (Side-Wall Access) and chapter 5 (Bottom-Face Access). Note that all light exiting the bottom-face must pass through the entire substrate thickness.

The bandgap of most semiconductors exhibits a redshift with increasing temperature. This trend in silicon carbide has been shown in [29]. Both main peaks undergo a redshift of peak wavelength when heated. In 4H-SiC, the temperature change from 0 K to 455 K (The highest temperature tested) corresponds to a bandgap shift of approximately 0.08 eV or 8 nm.[30] Evidence of this can be seen in Figure 5.2 where there is a small red-shift in the first peak when heated from 30 °C to 183 °C.

These two mechanisms could account for the shift of the first peak from the

expected value of 390 nm to 405 nm. Another possibility is a calibration error in the spectrometer, though the consistency in peak shifts between the two styles of sample preparation suggest this is not just a measurement error. Working under these assumptions, the 405 nm is a result of phonon assisted band-to-band transitions analogous to the 390 nm peak discussed in chapter 4.

5.2.2 Colour Shift

When the temperature of the device is increased independently of input power (applied current and voltage unchanged), the emission undergoes a blue-shift that is very apparent to the eye.

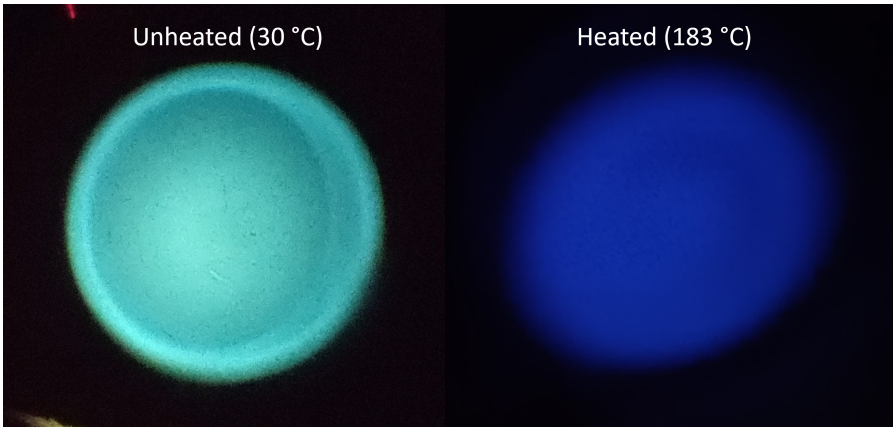

Figure 5.4: Emission of device viewed through an optical film with and without additional heating. The colour of the heated device appears as a much more intense violet when viewed in person as opposed to the deep blue picked up by the camera.

Figure 5.4 shows images of the emission and illustrates the extent of the shift. The light was passed through an optical film to enable pictures of the light without over saturating the camera sensor. The actual colour observed when heated is a deep violet that is reminiscent of ultraviolet 'black' lights. Since we see in the

spectrum that there is not an actual blue-shift of the peaks (If anything there is a slight red-shift due to the effect of increased temperature reducing bandgap), it is clear that the primary methods of emission remain the same and the colour shift is due to the relative change between the intensity of each peak when heated.

The first peak in Figure 5.2 is due to phonon-assisted recombination and increases when heated. At low temperatures we would expect to see very little phonon assisted recombination as there would be very few phonons present. As temperature increases, so do the amount of phonons present in the lattice. The increase in phonon concentration increases the probability that a phonon with the correct momentum is present to assist in recombination.

The broad green peak is due to dislocations/stacking faults and potentially surface states as in chapter 4. When heat is applied, the intensity of this peak decreases. One explanation for this decrease is that it is directly related to the increase of the first peak. When heat was added, the voltage/current applied to the device was not altered so the total amount of electrons injected into the device is constant. The phonon-assisted recombination pathway and the dislocation/defect recombination pathways are in competition and an increase in one, reduces the number of charge carriers available to the other. Since there is an increase in the first peak, we can assume that there is a reduced amount of carriers available to recombine and contribute to the second peak.

The previous explanation does not account for any temperature dependence of the second peak. The increase in temperature may reduce the intensity of the

second peak independently from the increase in the first peak. Between the non-heated and heated measurements, the peak intensity of the blue-green emission is reduced by ∼80% which is in agreement with the findings in [29].

Comparing the observed quenching to other 4H-SiC emission lines reported in literature, a number of similarities emerge. Egilsson *et al.* describe the low temperature D_1 dislocation emission at 427 nm, with quenching beginning at 100 K and an estimated activation energy of 57 meV.

Using this observation and a variation of Equation 2.3 we can estimate the how many phonons have energy of at least the activation energy E_i.

$$N_i = \frac{g_i}{\exp \frac{E_i}{kT} - 1} \tag{5.1}$$

E_i is the activation energy of the trap while g_i is the degeneracy of the energy state and is dependent on the number of atoms in the base unit cell of the material (21 for 4H-SiC).

Using the values reported in [31], we find that quenching was observed to begin when ∼2.8% of phonons reach the activation energy.

Doing the same for our results assuming an activation energy for the blue-green band of 0.220 eV as reported in [29], we find that ∼7.8% of phonons will have energy at least equal to the activation energy. If quenching begins at roughly 3%, then our observation of significant reduction in blue-green emission can be largely attributed to thermal quenching.

5.2.3 Conclusion

Heating of the junction causes a significant colour change from primarily blue-green (30 °C) to deep violet when heated to 183° (Figure 5.4). This shift in colour does not persist when external heating is removed implying that the shift is not due to the introduction or alteration/propagation of lattice defects. The spectrum consists of two major peaks, both of which show a dependence on temperature.

The first peak is centered around 405 nm and attributed to phonon-assisted band-to-band recombination that has been red-shifted due to passing through the die substrate before being measured. The intensity of this peak increases drastically when heated to 183 °C and becomes the dominant peak. This increase is attributed to an increased generation of thermal phonons which subsequently increase the probability of interaction with electrons.

The second peak is centered around 510 nm and attributed to lattice defects/dislocation and donor-acceptor recombination. When heated, the intensity is reduced by ∼80% at 183 °C. This reduction is largely due to the thermal quenching of defects and trap states responsible for direct recombination pathways. The other contribution to the reduction in this peak is the reduction of available carriers available due to the increase of phonon-assisted band-to-band recombination seen in the first peak.

Upon heating, both peaks exhibit the expected small red-shift and peak broadening characteristic of semiconductors.

It is expected that these trends would continue upon further heating as it has been reported that the intensity of the first peak continues to increase up to at

least 806 K [29]. Higher temperatures were not tested due to device/packaging limitations.

Chapter 6

Conclusion

In this work, different methods were explored as a means to alter the electroluminescent spectrum of a prefabricated diode. A device was etched to create a nanoporous layer on the sidewall, resulting in an increase in green emission. This increase is attributed to bipolar lateral diffusion causing carriers to flow and then recombine in the porous side layer where there is a much higher density of surface defects.This is the first time this has been demonstrated in silicon carbide. The resulting SiC device is an indirect gap electrically active junction with nanoporous sidewalls acting as a recombination pathway. The concept is applicable to a broad range of materials and the recombination pathway need not be the same material as the junction.

The effect of temperature on emission spectrum was also explored. When the temperature of the forward biased junction was increased independently from voltage and current by means of an external resistive heater, a dramatic shift in wavelength occurs from blue-green to deep violet. This shift is not permanent and

directly relates to the temperature of the device during operation. A combination of mechanisms are proposed. The emission at 405 nm is understood to be phonon-assisted band-to-band recombination and the increase upon heating is attributed to an increased generation of thermal phonons. The second emission is broad and centered around 510 nm and a result of lattice defects/dislocations and donor-acceptor recombination. The suppression of this peak when heated is likely a result of multiple effects. First, the increase in intensity of the 405 nm peak results in a reduction of carriers available to recombine at the defects. The second mechanism is the thermal quenching of defects and trap states responsible for direct recombination pathways. Both of the above mechanisms and trends are expected to continue past the temperature tested. The implication of this result is that temperature control is vital to any application utilizing phonon-assisted recombination as a primary source of light emission. This sensitivity to temperature in conjunction with active temperature control could allow tuning of emission spectrum to ensure variation between devices is less noticeable and also allow for on the fly correction of LED colour to ensure more consistent colour output across the devices' lifetime.

Silicon carbide has largely been phased out as a light emitting material due to efficiency and cost factors. Recently, there has been rapid maturation of silicon carbide fabrication spurred by the demand for power electronics. This may enable silicon carbide to once again become practical for niche light emitting applications.

Bibliography

[1] H. Round, A new electric discharge, *Electrical World*, vol. 49(6), 308, 1907.

[2] O. V. Losev, Luminous carborundum [silicon carbide] detector and detection with crystals, *Telegrafiya i Telefoniya bez Provodov*, vol. 44, 485–494, 1927.

[3] G. P. James Baird, *Semiconductor radiant diode*, Patent, 1962.

[4] T. M. Okon and J. R. Biard, The first practical led, *Edison Tech Center*, vol. 9, 2015.

[5] T. Bright, Efficient blue light-emitting diodes leading to bright and energy-saving white light sources, *Sci. Backgr. Nobel Prize Phys*, 1–9, 2014.

[6] S. Nakamura, T. M. T. Mukai, and M. S. M. Senoh, High-power gan pn junction blue-light-emitting diodes, *Japanese Journal of Applied Physics*, vol. 30(12A), L1998, 1991, ISSN: 1347-4065.

[7] J. Y. Tsao, M. H. Crawford, M. E. Coltrin, *et al.*, Toward smart and ultra-efficient solid-state lighting, *Advanced Optical Materials*, vol. 2(9), 809–836, 2014, ISSN: 2195-1071. DOI: https://doi.org/10.1002/adom.201400131. [Online]. Available: https://onlinelibrary.wiley.com/doi/abs/10.1002/adom.201400131.

[8] J. A. Edmond, H.-S. Kong, and C. H. Carter, Blue leds, uv photodiodes and high-temperature rectifiers in 6h-sic, *Physica.*, vol. 185(1-4), 453–460, 1993, ISSN: 0921-4526. DOI: 10.1016/0921-4526(93)90277-D.

[9] W. Lu, Y. Ou, E. M. Fiordaliso, *et al.*, White light emission from fluorescent sic with porous surface, *Scientific Reports*, vol. 7(1), 9798, 2017, ISSN: 2045-2322. DOI: 10.1038/s41598-017-10771-7. [Online]. Available: https://doi.org/10.1038/s41598-017-10771-7.

[10] R. Ekstein, *The creation of silicon carbide revolutionary semiconductor*, Web Page, 2017. [Online]. Available: https://eepower.com/technical-articles/the-creation-of-silicon-carbide-revolutionary-semiconductor/.

[11] M. D. P. Emilio, *What does the future hold for wide-bandgap devices?* Web Page, 2022. [Online]. Available: https://www.powerelectronicsnews.com/what-does-the-future-hold-for-wide-bandgap-devices/.

[12] *High withstand voltage (reverse voltage) characteristics of sic sbds*, Web Page, 2024. [Online]. Available: https://toshiba.semicon-storage.com/us/semiconductor/product/diodes/sic-schottky-barrier-diodes/articles/high-withstand-voltage-reverse-voltage-characteristics-of-sic-sbds.html.

[13] *Wolfspeed selects north carolina for world's largest silicon carbide materials facility | wolfspeed*, Web Page, 2022. [Online]. Available: https://www.wolfspeed.com/company/news-events/news/wolfspeed-selects-north-carolina-for-worlds-largest-silicon-carbide-materials-facility/.

[14] I. N. C. Wolfspeed, *Wolfspeed unveils world's largest sic wafer fab | wolfspeed*, Web Page, 2022. [Online]. Available: https://www.wolfspeed.com/company/news-events/news/wolfspeed-opens-the-worlds-largest-200mm-silicon-carbide-fab-enabling-highly-anticipated-device-production/.

[15] A. Kitai, *Principles of solar cells, LEDs and related devices: the role of the PN junction*. John Wiley & Sons, 2019, ISBN: 1119451027.

[16] R. Paschotta, *Phonons*, Encyclopedia. DOI: 10.61835/spa. [Online]. Available: https://www.rp-photonics.com/phonons.html.

[17] R. Edginton, S. Mattana, S. Caponi, *et al.*, Preparation of extracellular matrix protein fibers for brillouin spectroscopy, *Journal of visualized experiments : JoVE*, vol. 2016, 2016. DOI: 10.3791/54648.

[18] J. Pankove, *Optical Processes in Semiconductors*. Prentice-Hall, 1971, ISBN: 9780136380238. [Online]. Available: https://books.google.ca/books?id=zK7vAAAAMAAJ.

[19] Y. Shi, *Growth of 3C-SiC and Graphene for Solar Water-Splitting Application*. 2019, ISBN: 9789176850213. DOI: 10.3384/diss.diva-159100.

[20] S. Bawa, T. Zhang, L. Dow, S. Peter, and A. H. Kitai, Porous sic electroluminescence from p–i–n junction and a lateral carrier diffusion model, *Journal of Applied Physics*, vol. 129(4), 2021, ISSN: 0021-8979. DOI: 10.1063/5.0033243. [Online]. Available: https://doi.org/10.1063/5.0033243.

[21] *Corrosion resistance*, Web Page. [Online]. Available: https://www.gab-neumann.com/Corrosion-resistance-of-sintered-silicon-carbide.

[22] M.-G. Kang, H. J. Lezec, and F. Sharifi, Stable field emission from nanoporous silicon carbide, *Nanotechnology*, vol. 24(6), 065 201, 2013, ISSN: 0957-4484. DOI: 10.1088/0957-4484/24/6/065201. [Online]. Available: https://dx.doi.org/10.1088/0957-4484/24/6/065201.

[23] Y. Ke, R. P. Devaty, and W. J. Choyke, Comparative columnar porous etching studies on n-type 6h sic crystalline faces, *physica status solidi (b)*, vol. 245(7), 1396–1403, 2008, ISSN: 0370-1972. DOI: 10.1002/pssb.200844024. [Online]. Available: https://dx.doi.org/10.1002/pssb.200844024.

[24] *Delid and decap | semitracks*, Web Page. [Online]. Available: https://www.semitracks.com/reference-material/failure-and-yield-analysis/failure-analysis-package-level/delid-and-decap.php.

[25] A. Myllynen, T. Sadi, and J. Oksanen, Diffusion-driven gainp/gaas light-emitting diodes enhanced by modulation doping, *Optical and Quantum Electronics*, vol. 51(3), 90, 2019, ISSN: 1572-817X. DOI: 10.1007/s11082-019-1806-z. [Online]. Available: https://doi.org/10.1007/s11082-019-1806-z.

[26] I. Kim, P. Kivisaari, J. Oksanen, and S. Suihkonen, *Diffusion-driven charge transport in light emitting devices*, Electronic Article, 2017. DOI: 10.3390/ma10121421.

[27] G. Feng, J. Suda, and T. Kimoto, Triple shockley type stacking faults in 4h-sic epilayers, *Applied Physics Letters*, vol. 94(9), 091 910, 2009, ISSN: 0003-6951. DOI: 10.1063/1.3095508. [Online]. Available: https://dx.doi.org/10.1063/1.3095508.

[28] L. Lin, Y. Ou, V. Jokubavicius, *et al.*, An adhesive bonding approach by hydrogen silsesquioxane for silicon carbide-based led applications, *Materials Science in Semiconductor Processing*, vol. 91, 9–12, 2019. DOI: 10.1016/j.mssp.2018.10.028.

[29] A. M. Strel'chuk, E. V. Kalinina, and A. A. Lebedev, Temperature dependence of the band-edge injection electroluminescence of 4h-sic pn structure, *Materials Science Forum*, vol. 740-742, 569–572, 2013, ISSN: 1662-9752. DOI: 10.4028/www.scientific.net/MSF.740-742.569. [Online]. Available: https://www.scientific.net/MSF.740-742.569.

[30] E. Cannuccia and A. Gali, Thermal evolution of silicon carbide electronic bands, *Physical Review Materials*, vol. 4(1), 014 601, 2020, PRMATERIALS. DOI: 10.1103/PhysRevMaterials.4.014601. [Online]. Available: https://link.aps.org/doi/10.1103/PhysRevMaterials.4.014601.

[31] T. Egilsson, J. P. Bergman, I. G. Ivanov, A. Henry, and E. Janzén, Properties of the D_1 bound exciton in $4H-$SiC, *Physical Review B*, vol. 59(3), 1956–1963, 1999, PRB. DOI: 10.1103/PhysRevB.59.1956. [Online]. Available: https://link.aps.org/doi/10.1103/PhysRevB.59.1956.